International Journal of Control, Automation, and Systems 21(2) (2023) 630-644
http://dx.doi.org/10.1007/s12555-021-0823-4
ISSN:1598-6446 eISSN:2005-4092
http://www.springer.com/12555

Chattering-free Fast Fixed-time Sliding Mode Control for Uncertain Robotic Manipulators

Huayang Sai, Zhenbang Xu*, Enyang Zhang, Chunyang Han, and Yang Yu

Abstract: In this paper, we introduce a dynamic controller that dedicates fixed-time trajectory tracking for uncertain robotic manipulators. First, a new nonlinear function is designed and applied to the fixed-time sliding mode (FSM) surface. The derivative of the proposed nonlinear function is continuous, which can ensure the continuity and smoothness of the control torque, and it makes the sliding surface facilitate fast convergence rates of the system tracking error. Then, a FSM control scheme is designed using the proposed sliding mode surface. Combined the Lyapunov stability theory, we show that the proposed controller has fixed-time convergence independent of the initial state of the system. Moreover, the proposed control scheme is advantageous in that the control torque is continuous without transient change. This eliminates the chattering of uncertain robotic manipulators and makes the control torque smoother. Simulation results show that a faster error convergence rate can be obtained with a smaller control torque range. Finally, the above-mentioned effectiveness and superiority of the proposed control scheme are validated using simulations and experimental results.

Keywords: Fixed-time control, robotic manipulator, sliding mode control, trajectory tracking.

1. INTRODUCTION

Tracking control of robotic manipulators is attracting increasing interest in the field of robotic manipulator control. Various control schemes have been applied extensively to the trajectory-tracking control of robotic manipulators, such as proportional-integral-derivative control [1], fuzzy control [2], neural network control [3], and sliding mode control (SMC) [4-6]. However, considering the structural uncertainties and external disturbances, realizing accurate and fast-tracking control of robotic manipulators remains a major challenge.

Among various advanced control technologies, SMC has gained much attention, owing to its robustness and ease of implementation in uncertain environments. However, one major drawback of traditional SMC applications is chattering, which significantly affects the tracking control performance of robotic manipulators. Moreover, traditional SMC has the problem of asymptotic stability of the system when the time approaches infinity, but the system needs to converge in a limited time in many applications. To achieve finite-time convergence of the system state, a terminal sliding mode control (TSMC) algorithm has been proposed in [7]. As a finite-time control algorithm, TSMC guarantees the convergence of system states within finite time, after the states reach the manifold. In [8], a nonsingular terminal sliding mode control scheme is proposed to address the singularity problem of TSMC. A nonsingular fast terminal sliding mode control (NFTSMC) scheme has also been developed to realize rapid convergence of system states far from the origin [9]. Yu *et al.* [10] proposed a new form of TSMC with the advantages of high precision and chattering suppression. Van *et al.* [11] discussed finite-time fault-tolerant control of manipulators based on NFTSMC. Subsequently, a fast nonsingular integral TSMC scheme was designed by introducing a power integral term including the boundary-like structure to reduce chattering [12]. To estimate the coupling uncertainties, adaptive NFTSMC [13], adaptive second-order TSMC [14], and adaptive second-order NFTSMC [15] have been proposed in combination with adaptive technology.

Despite the above advancements, the prediction of the settling time depends on the initial state of the system.

Manuscript received September 26, 2021; revised February 21, 2022; accepted March 27, 2022. Recommended by Associate Editor Maolin Jin under the direction of Editor Kyoung Kwan Ahn. This work was partially supported by the National Natural Science Foundation of China (11972343).

Huayang Sai is with the CAS Key Laboratory of On-orbit Manufacturing and Integration for Space Optics System, Changchun Institute of Optics, Fine Mechanics and Physics, Chinese Academy of Sciences, Changchun 130033, China and University of Chinese Academy of Sciences, Beijing 100049, China (e-mail: saihuayang18@mails.ucas.ac.cn). Zhenbang Xu, Enyang Zhang, Chunyang Han, and Yang Yu is with the CAS Key Laboratory of On-orbit Manufacturing and Integration for Space Optics System, Changchun Institute of Optics, Fine Mechanics and Physics, Chinese Academy of Sciences, Changchun 130033, China (e-mails: xuzhenbang@ciomp.ac.cn, zhangenyangnuaa@126.com, hanchunyang.312@163.com, yuyang@ciomp.ac.cn).
* Corresponding author.

Thus, finite-time control has limited real-time application because the initial system conditions are usually unknown or difficult to obtain. In response, Polyakov [16] introduced a fixed-time control technology that can guarantee a bounded convergence time independent of initial states. Subsequently, detailed mathematical analyses of fixed-time stability and convergence are presented [17-19]. A distinctive feature of fixed-time control is that the settling time depends only on the defined parameters and is independent of the initial states. The upper bound of settling time of fixed-time stable systems was enhanced in the works of Gomez [20] and Aldana *et al*. [21]. In recent years, several fixed-time control algorithms based on SMC have been used for spacecraft attitude stability control [22-24] and second-order multiagent systems [25-27], owing to its superior characteristics.

Over the years, there have been serious efforts to explore fixed-time SMC in the field of robot control. Li *et al*. [28] proposed a multivariable fixed-time follower formation control scheme for a group of nonholonomic mobile robots. Jin [29] proposed an adaptive fixed-time control scheme using universal barrier functions to address the problem of asymmetric output constraint of robotic manipulators. By employing adaptive fuzzy control technique, a singularity-free fixed-time fuzzy controller was designed for the robotic manipulator system [30]. Su *et al*. [31] designed a new fixed-time sliding surface and applied it to trajectory tracking of robotic manipulators. However, the control torque produces transient changes, which results in discontinuous chattering of robotic manipulators, owing to the unsmooth sliding surface. Zhang *et al*. [32] designed a smooth fixed-time sliding surface for trajectory tracking of a robotic manipulator. Sai *et al*. [33] considered fixed-time convergence under saturation of the robotic manipulator actuator. However, they achieved a smooth sliding surface at the expense of the convergence rate. It is worth mentioning that suitable convergence rates are always realized at the expense of large control torque ranges in fixed-time SMC, which is a challenge with respect to actuators in robotic manipulators. Unfortunately, although some existing fixed-time controllers have been applied to robotic manipulators, the ranges of control torque are always ignored [29-32].

In this paper, we focused on the problem of discontinuous control torque and excessive control torque ranges in the fixed-time SMC for uncertain robotic manipulators. The main contributions of this paper are a novel fast continuous fixed-time sliding mode (FCFSM) surface and a fast continuous fixed-time SMC scheme for trajectory tracking of uncertain robotic manipulators. Two distinctive advantages of the proposed sliding mode surface are continuity and smoothness, which guarantee that the control torque does not change transiently, and the input control torque is chattering-free. Furthermore, the proposed approach can ensure a rapid convergence rate with a small control torque range, and the control scheme has good robustness and non-singularity for different initial states of the system over a range of control moments. The results of comparison with existing controllers via simulations and experimental results validate these characteristics of the proposed controller.

The remainder of this paper is organized as follows: Certain basic symbols, definitions, and dynamic models of the robotic manipulator are described in Section 2. The FCFSM control (FCFSMC) scheme and its stability analysis are presented in Section 3. In Section 4, the simulation results of the two sets in comparison to existing methods are presented and the experimental results are represented in Section 5. Finally, Section 6 summarizes the proposed control scheme and outlines future research directions.

2. PRELIMINARIES

2.1. Description of notations

In this paper, the norm of the matrix $\boldsymbol{A} \in \mathbb{R}^{n\times n}$ and vector $\boldsymbol{x} = \left[x_1, x_2, \cdots, x_n\right]^T$ are denoted as $\|\boldsymbol{A}\| = tr\left(\boldsymbol{A}^T\boldsymbol{A}\right)$ and $\|\boldsymbol{x}\| = \sqrt{\boldsymbol{x}^T\boldsymbol{x}}$, respectively, and diag $(\cdot)$ denotes a diagonal matrix. $\lambda_{\min}\{\boldsymbol{A}\}$ and $\lambda_{\max}\{\boldsymbol{A}\}$ are the minimum and maximum eigenvalues of the matrix $\boldsymbol{A}$, respectively. The nonlinear function $\text{sig}^{\alpha}(x)$ and vector $\mathbf{Sig}^{\alpha}(\boldsymbol{x}) \in \mathbb{R}^n$ can be written as

$$\text{sig}^{\alpha}(x) = |x|^{\alpha}\,\text{sgn}(x),\ (\alpha > 0), \tag{1}$$

$$\mathbf{Sig}^{\alpha}(\boldsymbol{x}) = \left[|x_1|^{\alpha}\,\text{sgn}(x_1)\cdots, |x_n|^{\alpha}\,\text{sgn}(x_n)\right]^T,\ (\alpha > 0), \tag{2}$$

where $\text{sgn}(x)$ is the signum function.

2.2. Some definitions and lemmas

For the following nonlinear system

$$\dot{\xi} = f(\xi),\ \xi(0) = \xi_0, \tag{3}$$

where $\xi \in \mathbb{R}^n$ is the system state and the function $f : \mathbb{R}^n \to \mathbb{R}^n$ is nonlinear, and the origin is assumed to be an equilibrium point of system (3). The following standard definitions and lemmas are used in this work.

Definition 1 (Global finite-time stability) [34]**:** The origin of (3) is globally finite-time stable if it is globally asymptotically stable and any solution of (3) reaches the equilibrium point at some finite time moment, i.e., $\forall t \geqslant T(\xi_0) : \xi(t, \xi_0) = 0$, where $T : \mathbb{R}^n \to \mathbb{R}_+ \cup \{0\}$ is called the settling-time function.

Definition 2 (Fixed-Time stability) [16,17]**:** The equilibrium point of the system in (3) is fixed-time stable, if it is globally finite-time stable, and the settling time is bounded. That is, $\exists T_{\max} > 0 : \forall \xi_0 \in \mathbb{R}^n$ and $T(\xi_0) \leqslant T_{\max}$.

Lemma 1 [16, Lemma 1]**:** For the system in (3), if there is a positive-definite continuous function $V(\xi)$:

$U \to \mathbb{R}^n$ and real numbers α, $\beta > 0$, $0 < p < 1$ and $q > 1$ that the inequality $\dot{V}(\xi) + \alpha V^p(\xi) + \beta V^q(\xi) < 0$, $\xi \in U \backslash \{0\}$ a reality, the system is globally fixed-time stable with a settling time T bounded by

$$T < T_{\max} = \frac{1}{\alpha(1-p)} + \frac{1}{\beta(q-1)}. \tag{4}$$

Lemma 2 [19, Lemma 3.4]**:** For $\xi_1, \xi_2, \cdots, \xi_N \geqslant 0$, the following inequality is satisfied

$$\sum_{i=1}^{N} \xi_i^p \geq \left(\sum_{i=1}^{N} \xi_i \right)^p \quad \text{if } 0 < p \leq 1, \tag{5}$$

$$\sum_{i=1}^{N} \xi_i^p \geq N^{1-p} \left(\sum_{i=1}^{N} \xi_i \right)^p \quad \text{if } 1 < p < \infty. \tag{6}$$

Lemma 3 [35]**:** If $f(x)$ and $g(x)$ are two continuous functions at $x_0 \in \mathbb{R}^n$, then the function $f(x) + g(x)$ is also continuous at x_0.

Lemma 4: For a positive constant α and $x \in \mathbb{R}$, the following equations hold

$$d|x|^{\alpha+1}/dx = (\alpha+1)|x|^{\alpha} \operatorname{sgn}(x), \tag{7}$$

$$d\left[|x|^{\alpha+1} \operatorname{sgn}(x)\right]/dx = (\alpha+1)|x|^{\alpha}. \tag{8}$$

The proof of Lemma 4 can be easily obtained by the limits of the derivative when $x \to 0^+$ and $x \to 0^-$.

2.3. Manipulator robotic dynamics model

We consider the dynamics of a general rigid robotic manipulator system with n-degrees-of-freedom given in [36],

$$\boldsymbol{M}(\boldsymbol{q})\ddot{\boldsymbol{q}} + \boldsymbol{C}(\boldsymbol{q},\dot{\boldsymbol{q}})\dot{\boldsymbol{q}} + \boldsymbol{G}(\boldsymbol{q}) = \boldsymbol{\tau} + \boldsymbol{\tau_d}, \tag{9}$$

where $\boldsymbol{q}, \dot{\boldsymbol{q}}, \ddot{\boldsymbol{q}} \in \mathbb{R}^n$ represent the generalized position, velocity, and acceleration vector of the robotic manipulator, respectively. $\boldsymbol{M}(\boldsymbol{q}) \in \mathbb{R}^{n\times n}$ is the symmetric and positive-definite inertia matrix, $\boldsymbol{C}(\boldsymbol{q},\dot{\boldsymbol{q}}) \in \mathbb{R}^{n\times n}$ is the centrifugal-Coriolis matrix, and $\boldsymbol{G}(\boldsymbol{q}) \in \mathbb{R}^n$ is the Cartesian gravitational term. $\boldsymbol{\tau}$ is the joint torque vector, and $\boldsymbol{\tau_d}$ is the bounded external disturbance. To track the trajectory of the robotic manipulator, the position-tracking error and speed tracking error are denoted as

$$\boldsymbol{e} = \boldsymbol{q} - \boldsymbol{q}_d,\ \dot{\boldsymbol{e}} = \dot{\boldsymbol{q}} - \dot{\boldsymbol{q}}_d, \tag{10}$$

where $\boldsymbol{q}_d, \dot{\boldsymbol{q}}_d \in \mathbb{R}^n$ denote the desired position and desired velocity, respectively. It is reasonable to postulate that the dynamics of robotic manipulators have the following properties:

Property 1 [37]**:** Generally, the matrices $\boldsymbol{M}(\boldsymbol{q}), \boldsymbol{C}(\boldsymbol{q},\dot{\boldsymbol{q}})$ and $\boldsymbol{G}(\boldsymbol{q})$ can be described as

$$\begin{cases} \boldsymbol{M}(\boldsymbol{q}) = \boldsymbol{M}_0(\boldsymbol{q}) + \Delta\boldsymbol{M}(\boldsymbol{q}), \\ \boldsymbol{C}(\boldsymbol{q},\dot{\boldsymbol{q}}) = \boldsymbol{C}_0(\boldsymbol{q},\dot{\boldsymbol{q}}) + \Delta\boldsymbol{C}(\boldsymbol{q},\dot{\boldsymbol{q}}), \\ \boldsymbol{G}(\boldsymbol{q}) = \boldsymbol{G}_0(\boldsymbol{q}) + \Delta\boldsymbol{G}(\boldsymbol{q}), \end{cases} \tag{11}$$

where $\boldsymbol{M}_0(\boldsymbol{q}), \boldsymbol{C}_0(\boldsymbol{q},\dot{\boldsymbol{q}})$, and $\boldsymbol{G}_0(\boldsymbol{q})$ are the nominal parts of the model parameters, and $\Delta\boldsymbol{M}(\boldsymbol{q})$, $\Delta\boldsymbol{C}(\boldsymbol{q},\dot{\boldsymbol{q}})$, and $\Delta\boldsymbol{G}(\boldsymbol{q})$ represent the system uncertainties.

Assumption 1 [37]**:** The matrices $\boldsymbol{M}(\boldsymbol{q})$, $\boldsymbol{C}(\boldsymbol{q},\dot{\boldsymbol{q}})$, and $\boldsymbol{G}(\boldsymbol{q})$ are bounded by

$$M_m \leqslant \|\boldsymbol{M}(\boldsymbol{q})\| \leqslant M_M, \text{ for } \forall \boldsymbol{q} \in \mathbb{R}^n, \tag{12}$$

$$\|\boldsymbol{C}(\boldsymbol{q},\dot{\boldsymbol{q}})\| \leqslant C_M \|\dot{\boldsymbol{q}}\|, \text{ for } \forall \boldsymbol{q},\dot{\boldsymbol{q}} \in \mathbb{R}^n, \tag{13}$$

$$\|\boldsymbol{G}(\boldsymbol{q})\| \leqslant G_M, \text{ for } \forall \boldsymbol{q} \in \mathbb{R}^n, \tag{14}$$

where M_m, M_M, C_M, and G_M are known positive constants.

3. DESIGN APPROACH FOR FAST CONTINUOUS FIXED-TIME SLIDING MODE CONTROL

3.1. FCFSM surface design

To ensure stability and transient performance of the control system, it is essential to design the SMC efficiently. We introduce a novel continuous nonlinear function $s^p(x)$ given by

$$s^p(x) = \begin{cases} |x|^p \operatorname{sgn}(x), & |x| \geqslant \delta, \\ l_1 x + l_2 x^2 \operatorname{sgn}(x) + l_3 x^3, & |x| < \delta, \end{cases} \tag{15}$$

where $x \in \mathbb{R}$ is the variable, and p and δ are two defined positive constants satisfying $0 < p < 1$ and $0 < \delta \leqslant 1$. l_1, l_2, and l_3 are constants defined as follows:

$$\begin{cases} l_1 = \left(\frac{1}{2}p^2 - \frac{5}{2}p + 3\right)\delta^{p-1}, \\ l_2 = \left(-p^2 + 4p - 3\right)\delta^{p-2}, \\ l_3 = \left(\frac{1}{2}p^2 - \frac{3}{2}p + 1\right)\delta^{p-3}. \end{cases} \tag{16}$$

The first and second derivatives of $s^p(x)$ with respect to x can be obtained easily by referring to Lemma 4, and we separately represent them by $f^p(x)$ and $g^p(x)$ as

$$f^p(x) = s^{p\prime}(x) = \begin{cases} p|x|^{p-1}, & |x| \geqslant \delta, \\ l_1 + 2l_2|x| + 3l_3x^2, & |x| < \delta, \end{cases} \tag{17}$$

$$g^p(x) = s^{p\prime\prime}(x) = \begin{cases} p(p-1)|x|^{p-2} \operatorname{sgn}(x), & |x| \geqslant \delta, \\ 2l_2 \operatorname{sgn}(x) + 6l_3x, & |x| < \delta. \end{cases} \tag{18}$$

Considering $\delta = 0.01$ and $p = 0.5$, the nonlinear function $s^p(x)$ and its first and second derivatives can be depicted as in Fig. 1. It can be shown that the functions $s^p(x)$ and $s^{p\prime}(x)$ are continuous for $x \in \mathbb{R}$ and $s^{p\prime\prime}(x)$ is continuous for $x \in \mathbb{R}\backslash\{0\}$. Therefore, $s^p(x)$ is continuous and smooth for $x \in \mathbb{R}$, and $s^{p\prime}(x)$ is continuous and smooth for $x \in \mathbb{R}\backslash\{0\}$. Moreover, the nonlinear function $s^p(x)$ has a large slope when variable x goes into small sets near zero.

For the nonlinear function $s^p(x)$, the value of p has a strong influence on its slope. In Fig. 2, as the value of p decreases, the slope of function $s^p(x)$ increases rapidly when

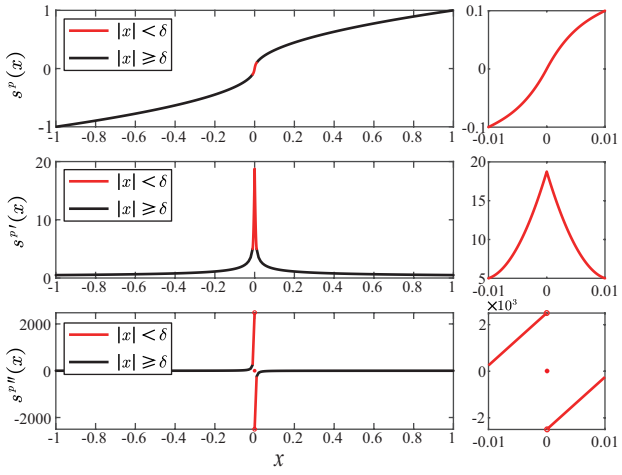

Fig. 1. Variation of $s^p(x)$ and the first and second derivatives of $s^p(x)$ with x.

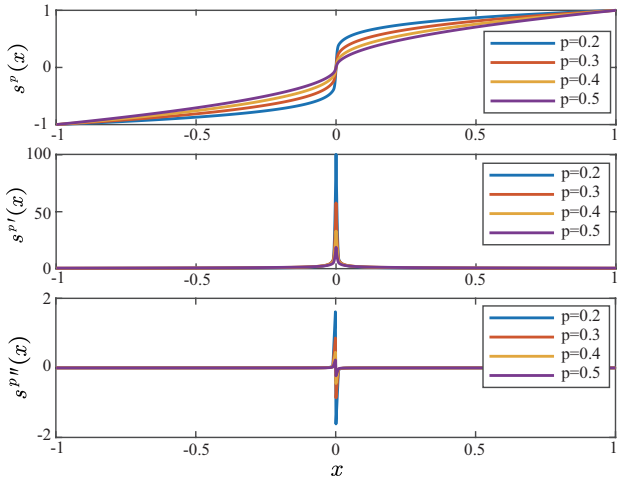

Fig. 2. $s^p(x)$, and the first and second derivatives of $s^p(x)$ for different p.

x goes to zero, and it can remain continuous and smooth. In other words, the convergence rate can be accelerated by decreasing the value of p, without any concern regarding changing the properties of function $s^p(x)$.

Then, we define the nonlinear function $s^q(x)$ as

$$s^q(x) = \mathrm{sig}^q(x), \tag{19}$$

where q is a positive constant with $q > 1$. For the nonlinear function $s^q(x)$, the first derivative with respect to x can be written as

$$h^q(x) = s^{q\prime}(x) = q|x|^{q-1}. \tag{20}$$

The graphs of functions $s^q(x)$ and $s^{q\prime}(x)$ are shown in Fig. 3, where it can be seen that $s^q(x)$ is continuous and smooth for $x \in \mathbb{R}$, and $s^{q\prime}(x)$ is continuous and smooth for $x \in \mathbb{R}\backslash\{0\}$. When variable x is far from the origin, the slope of

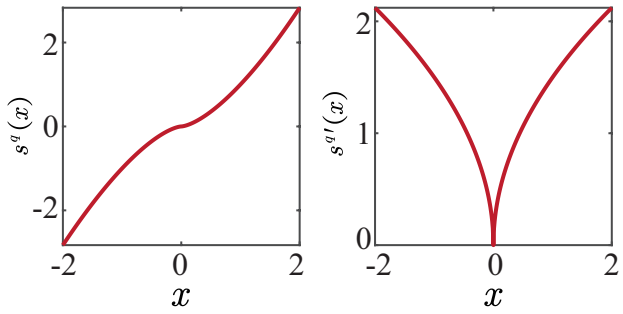

Fig. 3. Plots of $s^q(x)$ and $s^{q\prime}(x)$ with x.

$s^q(x)$ increases rapidly and reaches zero when the variable x is close to zero.

To simplify the design and analysis of the controller, the following vectors are defined

$$\boldsymbol{S}^p(\boldsymbol{x}) = [s^p(x_1), \cdots, s^p(x_n)]^T, \tag{21}$$
$$\boldsymbol{F}^p(\boldsymbol{x}) = \mathrm{diag}(f^p(x_1), \cdots, f^p(x_n)), \tag{22}$$
$$\boldsymbol{S}^q(\boldsymbol{x}) = [s^q(x_1), \cdots, s^q(x_n)]^T, \tag{23}$$
$$\boldsymbol{H}^q(\boldsymbol{x}) = \mathrm{diag}(h^q(x_1), \cdots, h^q(x_n)), \tag{24}$$

where the nonlinear function $s^p(x)$ is defined in (15) and its first derivative $f^p(x)$ is denoted in (17). The nonlinear function $s^q(x)$ is defined in (19) and its first derivative $h^q(x)$ is denoted in (20). As defined in the function, p and q are two positive constants with $0 < p < 1$ and $q > 1$, and n represents the dimension of the vector.

Based on the vectors $\boldsymbol{S}^p(\boldsymbol{x})$ and $\boldsymbol{S}^q(\boldsymbol{x})$, a novel FCFSM surface is designed as

$$\boldsymbol{s} = \dot{\boldsymbol{e}} + \boldsymbol{K}_1\boldsymbol{S}^p(\boldsymbol{e}) + \boldsymbol{K}_2\boldsymbol{S}^q(\boldsymbol{e}), \tag{25}$$

where $\boldsymbol{e}$ is the vector of the position tracking error, and $\boldsymbol{K}_1, \boldsymbol{K}_2 \in \mathbb{R}^{n\times n}$ are two defined positive definite symmetric matrices.

Remark 1: Since $s^p(x)$ and $s^q(x)$ are both continuous and smooth functions, according to Lemma 3, the FCFSM surface is also continuous and smooth.

Remark 2: When the system state is close to the origin, $\boldsymbol{K}_1\boldsymbol{S}^p(\boldsymbol{e})$ dominates $\boldsymbol{K}_2\boldsymbol{S}^q(\boldsymbol{e})$. When the system state is far from the origin, $\boldsymbol{K}_2\boldsymbol{S}^q(\boldsymbol{e})$ dominates the fixed-time convergence rate. Hence, the FCFSM surface can always maintain fast convergence.

3.2. FCFSM surface analysis and comparison

In this section, the advantages of the proposed sliding surface will be explained by comparison. Two similar sliding surfaces have been proposed previously: fixed-time terminal sliding mode (Fixed TSM) surface in [31] and singularity-free fixed-time sliding mode (SFSM) surface in [32]. To verify the fast convergence of our proposed FCFSM surface, the error convergence rates are compared

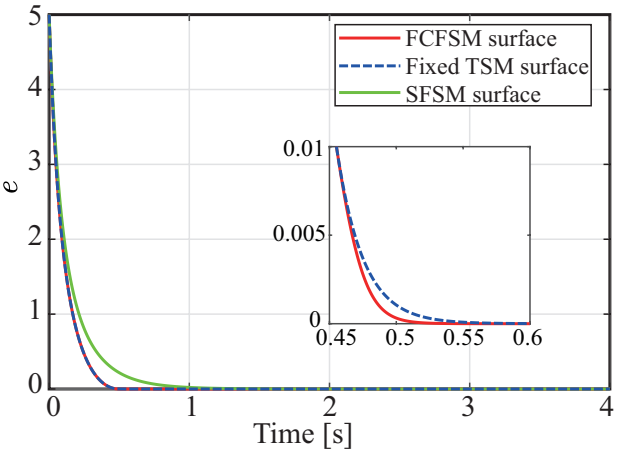

Fig. 4. Convergence rates with different sliding mode surfaces.

with those of the Fixed TSM surface and SFSM surface. The Fixed TSM surface in [31] can be expressed as

$$s_1^p(x) = \begin{cases} |x|^p \operatorname{sgn}(x), & |x| \geqslant \delta_1, \\ \delta_1^{p-1} x, & |x| < \delta_1, \end{cases} \tag{26}$$

$$s_1 = \dot{e} + K_1 s_1^p(x) + K_2 \operatorname{sig}^q(e), \tag{27}$$

where $0 < p < 1$, $q > 1$, $0 < \delta_1 \leqslant 1$, $K_1, K_2 \in \mathbb{R}$ are two known positive constants.

The SFSM surface in [32] can be expressed as

$$s_2^p(x) = \begin{cases} \operatorname{sig}^{1-\delta_2}(x), & |x| \geqslant \delta_2, \\ \dfrac{-1-\ln\delta_2}{1-\delta_2-\delta_2\ln\delta_2}\operatorname{sig}^{2-\delta_2}(x) \\ \quad + \dfrac{\delta_2^{-2\delta_2}}{1-\delta_2-\delta_2\ln\delta_2}\delta_2^{|x|}x, & |x| < \delta_2, \end{cases} \tag{28}$$

$$s_2 = \dot{e} + K_1 s_2^p(e) + K_2 \operatorname{sig}^q(e), \tag{29}$$

where $q > 1$, $\delta_2 \in (0, \exp(-1))$, K_1, $K_2 \in \mathbb{R}$ are two known positive constants.

With reference to the works of Su *et al.* [31] and Zhang *et al.* [32], the parameters are selected as $p = 0.5$, $q = 1.5$, $\delta_1 = 0.01$, $\delta_2 = 0.3$, $K_1 = K_2 = 2$. The initial state is defined as $e(0) = 5$, and the simulation results with different sliding mode surfaces are shown in Fig. 4. As shown in Fig. 4, the convergence rate of the FCFSM surface is faster than that of the Fixed TSM surface when $e < 0.01$, and they are both faster than the SFSM surface with the reduction of convergence error. In particular, the convergence rate of the SFSM surface decreases rapidly when $e < 1$.

Remark 3: Function $s_1^p(x)$ and the proposed nonlinear function $s^p(x)$ have similar properties, especially when $|x| \geqslant \delta$, it has $s_1^p(x) = s^p(x)$. Therefore, refer to the work of Su *et al.* [31] and define $\delta_1 = \delta = 0.01$. Function $s_2^p(x)$ does not contain parameter p, the purpose is to distinguish

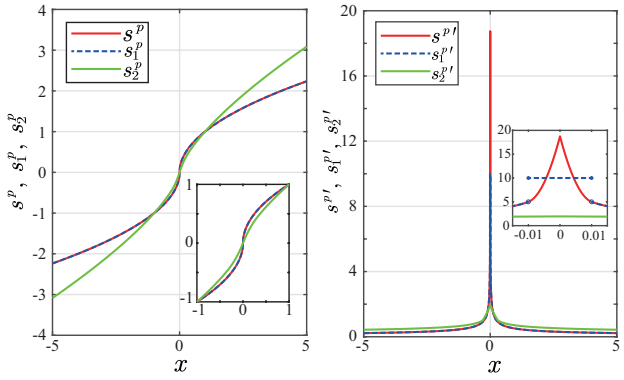

Fig. 5. Comparison of different nonlinear functions $s^p(x), s_1^p(x), s_2^p(x)$ and their first derivatives.

the sliding mode surface s_2. When the system error is close to zero, small δ_2 hinders the rapid convergence of the system error. Considering the work of Zhang *et al.* [32], we set δ_2 as 0.3.

To explain the difference in the error convergence rate, the nonlinear functions $s^p(x)$, $s_1^p(x)$, $s_2^p(x)$ and their first derivatives are shown in Fig. 5. As can be seen in Fig. 5, the value of $s_2^{p\prime}(x)$ is much smaller than that of $s^{p\prime}(x)$ and $s_1^{p\prime}(x)$ when $|x| < 0.01$. This means that the convergence rate of SFSM surface is slower than that of the other two sliding surfaces when x is close to the origin. The value of $s^{p\prime}(x)$ is approximately twice that of $s_1^{p\prime}(x)$ when x goes to zero. Thus, the error converges to the origin faster in the FCFSM surface than in the Fixed TSM surface. Moreover, there are some remarks that need to be noted.

Remark 4: When the tracking error is large, the sliding surface is expected to provide a small convergence rate to ensure a small control torque of the system. When the tracking error is small, the sliding surface is expected to provide a large convergence rate to ensure a fast convergence rate. From Fig. 5, it can be seen that the proposed nonlinear function $s^p(x)$ can make the sliding mode surface satisfy the above properties.

Remark 5: $s_1^{p\prime}(x)$ is discontinuous at $x = \delta_1 = 0.01$, which may lead to discontinuous acceleration and cause the system chattering.

Remark 6: The value of $s_2^p(x)$ is larger than that of $s^p(x)$ and $s_1^p(x)$ for the high value of $|x|$, which may lead to a large initial control torque when the initial convergence error is large.

3.3. FCFSMC design

Based on the FCFSM surface, the FCFSMC scheme is designed as

$$\boldsymbol{\tau} = \boldsymbol{\tau}_0 + \boldsymbol{\tau}_1 + \boldsymbol{\tau}_2, \tag{30}$$

$$\boldsymbol{\tau}_0 = \boldsymbol{M}_0(\boldsymbol{q})\ddot{\boldsymbol{q}}_d + \boldsymbol{C}_0(\boldsymbol{q}, \dot{\boldsymbol{q}})\dot{\boldsymbol{q}} + \boldsymbol{G}_0(\boldsymbol{q}), \tag{31}$$

$$\boldsymbol{\tau}_1 = -\boldsymbol{K}_0 \mathbf{Sig}^r(\boldsymbol{s})$$

$$-\boldsymbol{M}_0(\boldsymbol{q})\left(\boldsymbol{K}_1\boldsymbol{F}^p(\boldsymbol{e})+\boldsymbol{K}_2\boldsymbol{H}^q(\boldsymbol{e})\right)\dot{\boldsymbol{e}}, \tag{32}$$

$$\boldsymbol{\tau}_2=-\frac{\boldsymbol{s}}{\|\boldsymbol{s}\|}u, \tag{33}$$

$$u=\frac{1}{1-\gamma}\left(k+b_0+b_1\|q\|+b_2\|\dot{q}\|^2+\gamma\|\boldsymbol{\tau}_0+\boldsymbol{\tau}_1\|\right), \tag{34}$$

where $\boldsymbol{K}_0\in\mathbb{R}^{n\times n}$ is a known positive-definite symmetric matrix, $r>1$ and $k>0$ are two positive gains. b_0, b_1, b_2 and γ are positive constants, and γ is given by

$$\gamma=\frac{m_2-m_1}{m_2+m_1}, \tag{35}$$

where m_1 and m_2 are two known positive constants satisfying

$$m_1\leqslant\left\|\boldsymbol{M}^{-1}(\boldsymbol{q})\right\|\leqslant m_2. \tag{36}$$

Remark 7: According to the above discussion, both $f^p(x)$ and $h^q(x)$ are continuous functions. Combined with Lemma 3, $\boldsymbol{K}_1\boldsymbol{F}^p(\boldsymbol{e})+\boldsymbol{K}_2\boldsymbol{H}^q(\boldsymbol{e})$ in (32) is also continuous. Then, it can be concluded that the control torque $\boldsymbol{\tau}$ in (30) is continuous.

Remark 8: For the sliding mode control method, it forces the tracking error to approach the sliding mode surface, and then reaches the origin along the sliding mode surface.

3.4. Stability analysis of the control system

Before demonstration of the convergence time of the control system, one important theorem is to be explained.

Theorem 1: In view of (9) and (11), the coupled uncertainty includes the external disturbance and system uncertainties. Thus, the coupled uncertainty $\boldsymbol{\rho}(t)$ can be written as

$$\boldsymbol{\rho}(t)=-\Delta\boldsymbol{M}(\boldsymbol{q})\ddot{\boldsymbol{q}}-\Delta\boldsymbol{C}(\boldsymbol{q},\dot{\boldsymbol{q}})\dot{\boldsymbol{q}}-\Delta\boldsymbol{G}(\boldsymbol{q})+\boldsymbol{\tau}_{\boldsymbol{d}}, \tag{37}$$

which can be bounded as

$$\|\boldsymbol{\rho}(t)\|<b_0+b_1\|\boldsymbol{q}(t)\|+b_2\|\dot{\boldsymbol{q}}(t)\|^2+\gamma\|\boldsymbol{\tau}\|. \tag{38}$$

Proof: According to (9) and (11), $\Delta\boldsymbol{M}(\boldsymbol{q})\ddot{\boldsymbol{q}}$ can be written as

$$\Delta\boldsymbol{M}(\boldsymbol{q})\ddot{\boldsymbol{q}}=\boldsymbol{E}\left(\boldsymbol{\tau}-\boldsymbol{C}(\boldsymbol{q},\dot{\boldsymbol{q}})-\boldsymbol{G}(\boldsymbol{q})+\boldsymbol{\tau}_{\boldsymbol{d}}\right), \tag{39}$$

where $\boldsymbol{E}\in\mathbb{R}^{n\times n}$ can be denoted as

$$\boldsymbol{E}\triangleq\boldsymbol{I}_{\boldsymbol{n}}-\boldsymbol{M}_0(\boldsymbol{q})\boldsymbol{M}^{-1}(\boldsymbol{q}). \tag{40}$$

Then, $\boldsymbol{M}_0(\boldsymbol{q})$ can be chosen as [38-40]

$$\boldsymbol{M}_0(\boldsymbol{q})=\frac{2}{m_1+m_2}\boldsymbol{I}_{\boldsymbol{n}}, \tag{41}$$

where m_1 and m_2 are two positive constants in (36).

Then, $\boldsymbol{E}$ can be derived as

$$\begin{aligned}\|\boldsymbol{E}\|&=\left\|\frac{(m_1+m_2)\boldsymbol{I}_{\boldsymbol{n}}-2\boldsymbol{M}^{-1}(\boldsymbol{q})}{m_1+m_2}\right\|\\&=\frac{\left\|\left(m_2\boldsymbol{I}_{\boldsymbol{n}}-\boldsymbol{M}^{-1}(\boldsymbol{q})\right)-\left(\boldsymbol{M}^{-1}(\boldsymbol{q})-m_1\boldsymbol{I}_{\boldsymbol{n}}\right)\right\|}{m_1+m_2}\\&\leqslant\frac{\left\|\left(m_2\boldsymbol{I}_{\boldsymbol{n}}-\boldsymbol{M}^{-1}(\boldsymbol{q})\right)+\left(\boldsymbol{M}^{-1}(\boldsymbol{q})-m_1\boldsymbol{I}_{\boldsymbol{n}}\right)\right\|}{m_1+m_2}\\&=\frac{m_2-m_1}{m_1+m_2}\triangleq\gamma<1.\end{aligned} \tag{42}$$

Therefore, the upper bound of the coupled uncertainty $\boldsymbol{\rho}(t)$ can be calculated as

$$\begin{aligned}\|\boldsymbol{\rho}(t)\|&=\|\Delta\boldsymbol{M}(\boldsymbol{q})\ddot{\boldsymbol{q}}+\Delta\boldsymbol{C}(\boldsymbol{q},\dot{\boldsymbol{q}})\dot{\boldsymbol{q}}+\Delta\boldsymbol{G}(\boldsymbol{q})-\boldsymbol{\tau}_{\boldsymbol{d}}\|\\&=\|\boldsymbol{E}\left(\boldsymbol{\tau}-\boldsymbol{C}(\boldsymbol{q},\dot{\boldsymbol{q}})-\boldsymbol{G}(\boldsymbol{q})+\boldsymbol{\tau}_{\boldsymbol{d}}\right)\\&\quad+\Delta\boldsymbol{C}(\boldsymbol{q},\dot{\boldsymbol{q}})\dot{\boldsymbol{q}}+\Delta\boldsymbol{G}(\boldsymbol{q})-\boldsymbol{\tau}_{\boldsymbol{d}}\|\\&<b_0+b_1\|\boldsymbol{q}(t)\|+b_2\|\dot{\boldsymbol{q}}(t)\|^2+\gamma\|\boldsymbol{\tau}\|.\end{aligned} \tag{43}$$

The proof is completed. □

Remark 9: Different from the upper bound of manipulator coupling uncertainty in [31], the proof in Theorem 1 is more rigorous due to the influence of manipulator joint angle is considered.

Theorem 2: Given the uncertain robotic manipulator system by (9) and the FCFSMC scheme proposed in (30)-(34), the trajectory tracking error of the manipulator system globally converges to an arbitrary small set δ of the origin with the settling time T and then goes to zero exponentially. The upper bound of the settling time $T_{\max}$ includes the reaching time T_r and the sliding time T_s. The reaching time T_r denotes the period in which the tracking trajectory converges globally to the sliding mode surface, and the sliding time T_s denotes the period in which the tracking trajectory error converges to an arbitrarily small domain of the origin. T, T_r and T_s are given by

$$T\leqslant T_{\max}=T_r+T_s, \tag{44}$$

$$\begin{aligned}T_r\leqslant&\frac{2}{k(m_1+m_2)^{\frac{1}{2}}}\\&+\frac{2}{n^{\frac{1-r}{2}}\lambda_{\min}(\boldsymbol{K}_0)(m_1+m_2)^{\frac{r+1}{2}}(r-1)},\end{aligned} \tag{45}$$

$$T_s\leqslant\frac{2^{\frac{1-p}{2}}}{(1-p)\lambda_{\min}(\boldsymbol{K}_1)}+\frac{\left(\frac{2}{n}\right)^{\frac{1-q}{2}}}{(q-1)\lambda_{\min}(\boldsymbol{K}_2)}. \tag{46}$$

Proof: The stability analysis of the proposed FCFSMC can be divided into the reaching phase and the sliding phase.

Step 1 (Stability and settling time analysis in reaching phase)**:**

Considering the sliding mode surface (25) and (9), (11), and (37), we can obtain

$$\boldsymbol{M}_0(\boldsymbol{q})\dot{\boldsymbol{s}}$$

$$
\begin{aligned}
&= \boldsymbol{M}_0(\boldsymbol{q})\left(\ddot{\boldsymbol{e}} + \left(\boldsymbol{K}_1\boldsymbol{F}^p(\boldsymbol{e}) + \boldsymbol{K}_2\boldsymbol{H}^q(\boldsymbol{e})\right)\dot{\boldsymbol{e}}\right)\\
&= \boldsymbol{M}_0(\boldsymbol{q})\left(\ddot{\boldsymbol{q}} - \ddot{\boldsymbol{q}}_d\right)\\
&\quad + \boldsymbol{M}_0(\boldsymbol{q})\left[\boldsymbol{K}_1\boldsymbol{F}^p(\boldsymbol{e}) + \boldsymbol{K}_2\boldsymbol{H}^q(\boldsymbol{e})\right]\dot{\boldsymbol{e}}\\
&= \boldsymbol{\tau} + \boldsymbol{\tau}_{\boldsymbol{d}} - \boldsymbol{\Delta M}_0(\boldsymbol{q})\ddot{\boldsymbol{q}} - \boldsymbol{\Delta C}(\boldsymbol{q},\dot{\boldsymbol{q}})\dot{\boldsymbol{q}}\\
&\quad - \boldsymbol{\Delta G}(\boldsymbol{q}) - \boldsymbol{C}_0(\boldsymbol{q},\dot{\boldsymbol{q}})\dot{\boldsymbol{q}} - \boldsymbol{G}_0(\boldsymbol{q}) - \boldsymbol{M}_0(\boldsymbol{q})\ddot{\boldsymbol{q}}_d\\
&\quad + \boldsymbol{M}_0(\boldsymbol{q})\left[\boldsymbol{K}_1\boldsymbol{F}^p(\boldsymbol{e}) + \boldsymbol{K}_2\boldsymbol{H}^q(\boldsymbol{e})\right]\dot{\boldsymbol{e}}\\
&= \boldsymbol{\tau} + \boldsymbol{\rho} - \boldsymbol{C}_0(\boldsymbol{q},\dot{\boldsymbol{q}})\dot{\boldsymbol{q}} - \boldsymbol{G}_0(\boldsymbol{q}) - \boldsymbol{M}_0(\boldsymbol{q})\ddot{\boldsymbol{q}}_d\\
&\quad + \boldsymbol{M}_0(\boldsymbol{q})\left[\boldsymbol{K}_1\boldsymbol{F}^p(\boldsymbol{e}) + \boldsymbol{K}_2\boldsymbol{H}^q(\boldsymbol{e})\right]\dot{\boldsymbol{e}}\\
&= -\frac{\boldsymbol{s}}{\|\boldsymbol{s}\|}\frac{1}{1-\gamma}\Big(k + b_0 + b_1\|\boldsymbol{q}\| + b_2\|\dot{\boldsymbol{q}}\|^2\\
&\quad + \gamma\|\boldsymbol{\tau}_0 + \boldsymbol{\tau}_1\|\Big) + \boldsymbol{\rho} - \boldsymbol{K}_0\mathbf{Sig}^r(\boldsymbol{s}).
\end{aligned}
\tag{47}
$$

We define the following Lyapunov function as

$$
V_1 = \frac{1}{2}\boldsymbol{s}^T\boldsymbol{M}_0(\boldsymbol{q})\boldsymbol{s}. \tag{48}
$$

Differentiating V_1 with respect to time yields

$$
\begin{aligned}
\dot{V}_1 &= \boldsymbol{s}^T\boldsymbol{M}_0(\boldsymbol{q})\dot{\boldsymbol{s}}\\
&= \boldsymbol{s}^T\begin{bmatrix} -\frac{\boldsymbol{s}}{\|\boldsymbol{s}\|}\frac{1}{1-\gamma}\begin{pmatrix} k + b_0 + b_1\|\boldsymbol{q}\| + b_2\|\dot{\boldsymbol{q}}\|^2 \\ +\gamma\|\boldsymbol{\tau}_0 + \boldsymbol{\tau}_1\| \end{pmatrix} \\ +\boldsymbol{\rho} - \boldsymbol{K}_0\mathbf{Sig}^r(\boldsymbol{s}) \end{bmatrix}\\
&= -\frac{\|\boldsymbol{s}\|}{1-\gamma}\left(k + b_0 + b_1\|\boldsymbol{q}\| + b_2\|\dot{\boldsymbol{q}}\|^2 + \gamma\|\boldsymbol{\tau}_0 + \boldsymbol{\tau}_1\|\right)\\
&\quad + \boldsymbol{s}^T\boldsymbol{\rho} - \boldsymbol{s}^T\boldsymbol{K}_0\mathbf{Sig}^r(\boldsymbol{s}).
\end{aligned}
\tag{49}
$$

Substituting (34) into (49) leads to

$$
\begin{aligned}
\dot{V}_1 &\leqslant -\gamma\|\boldsymbol{s}\|u - \|\boldsymbol{s}\|\begin{pmatrix} k + b_0 + b_1\|\boldsymbol{q}\| \\ +b_2\|\dot{\boldsymbol{q}}\|^2 + \gamma\|\boldsymbol{\tau}_0 + \boldsymbol{\tau}_1\| \end{pmatrix}\\
&\quad + \boldsymbol{s}^T\boldsymbol{\rho} - \boldsymbol{s}^T\boldsymbol{K}_0\mathbf{Sig}^r(\boldsymbol{s})\\
&\leqslant -\gamma\|\boldsymbol{s}\|u - \|\boldsymbol{s}\|\begin{pmatrix} k + b_0 + b_1\|\boldsymbol{q}\| \\ +b_2\|\dot{\boldsymbol{q}}\|^2 + \gamma\|\boldsymbol{\tau}_0 + \boldsymbol{\tau}_1\| \end{pmatrix}\\
&\quad + \|\boldsymbol{s}\|\|\boldsymbol{\rho}\| - \boldsymbol{s}^T\boldsymbol{K}_0\mathbf{Sig}^r(\boldsymbol{s}).
\end{aligned}
\tag{50}
$$

Combining the upper bound of the coupled uncertainty in (38) yields

$$
\begin{aligned}
\dot{V}_1 &\leqslant -\gamma\|\boldsymbol{s}\|u - \|\boldsymbol{s}\|\begin{pmatrix} k + b_0 + b_1\|\boldsymbol{q}\| \\ +b_2\|\dot{\boldsymbol{q}}\|^2 + \gamma\|\boldsymbol{\tau}_0 + \boldsymbol{\tau}_1\| \end{pmatrix}\\
&\quad + \|\boldsymbol{s}\|\begin{pmatrix} b_0 + b_1\|\boldsymbol{q}(t)\| \\ +b_2\|\dot{\boldsymbol{q}}(t)\|^2 + \gamma\|\boldsymbol{\tau}\| \end{pmatrix} - \boldsymbol{s}^T\boldsymbol{K}_0\mathbf{Sig}^r(\boldsymbol{s})\\
&= -\gamma\|\boldsymbol{s}\|u - k\|\boldsymbol{s}\| - \gamma\|\boldsymbol{s}\|\|\boldsymbol{\tau}_0 + \boldsymbol{\tau}_1\|\\
&\quad + \gamma\|\boldsymbol{s}\|\|\boldsymbol{\tau}\| - \boldsymbol{s}^T\boldsymbol{K}_0\mathbf{Sig}^r(\boldsymbol{s}).
\end{aligned}
\tag{51}
$$

It can be clearly seen that

$$
\|\boldsymbol{\tau}\| \leqslant \|\boldsymbol{\tau}_0 + \boldsymbol{\tau}_1\| + \|\boldsymbol{\tau}_2\|. \tag{52}
$$

Substituting (52) into (51), we have

$$
\begin{aligned}
\dot{V}_1 &\leqslant -\gamma\|\boldsymbol{s}\|u + \gamma\|\boldsymbol{s}\|\|\boldsymbol{\tau}_2\| - k\|\boldsymbol{s}\| - \boldsymbol{s}^T\boldsymbol{K}_0\mathbf{Sig}^r(\boldsymbol{s})\\
&= -k\|\boldsymbol{s}\| - \boldsymbol{s}^T\boldsymbol{K}_0\mathbf{Sig}^r(\boldsymbol{s})\\
&= -\sum_{i=1}^{n} k_{0i}|s_i|^{r+1} - k\|\boldsymbol{s}\|\\
&= -\lambda_{\min}(\boldsymbol{K}_0)\sum_{i=1}^{n}|s_i|^{r+1} - k\|\boldsymbol{s}\|\\
&= -\lambda_{\min}(\boldsymbol{K}_0)\left(\sum_{i=1}^{n}|s_i|^2\right)^{\frac{r+1}{2}} - k\|\boldsymbol{s}\|.
\end{aligned}
\tag{53}
$$

According to Lemma 2, (53) can be written as

$$
\begin{aligned}
&\dot{V}_1 \leqslant -n^{\frac{1-r}{2}}\lambda_{\min}(\boldsymbol{K}_0)\|\boldsymbol{s}\|^{r+1} - k\|\boldsymbol{s}\|\\
&\Rightarrow \dot{V}_1 + n^{\frac{1-r}{2}}\lambda_{\min}(\boldsymbol{K}_0)(m_1 + m_2)^{\frac{r+1}{2}}V^{\frac{r+1}{2}}\\
&\quad + kV^{\frac{1}{2}}(m_1 + m_2)^{\frac{1}{2}} \leqslant 0.
\end{aligned}
\tag{54}
$$

As described in Lemma 1 and Definition 2, V_1 is globally fixed-time stable, with the reaching time T_r bounded by (45).

Step 2 (Stability and settling time analysis in the sliding phase)**:**

The error convergence enters the sliding phase once the sliding surface reaches $s = 0$, and (25) can be written as follows:

$$
\dot{\boldsymbol{e}} = -\boldsymbol{K}_1\boldsymbol{S}^p(\boldsymbol{e}) - \boldsymbol{K}_2\boldsymbol{S}^q(\boldsymbol{e}). \tag{55}
$$

Since $s^p(e)$ is a piecewise function of e, there are two cases for discussion.

Case 1: If $\|\boldsymbol{e}\| \geqslant \delta$, (55) can be expressed as

$$
\dot{\boldsymbol{e}} = -\boldsymbol{K}_1\mathbf{Sig}^p(\boldsymbol{e}) - \boldsymbol{K}_2\mathbf{Sig}^q(\boldsymbol{e}). \tag{56}
$$

The following Lyapunov function is considered:

$$
V_2 = \frac{1}{2}\boldsymbol{e}^T\boldsymbol{e}. \tag{57}
$$

Taking the first derivative of (57), we have

$$
\begin{aligned}
\dot{V}_2 &= \boldsymbol{e}^T\dot{\boldsymbol{e}}\\
&= -\boldsymbol{e}^T\boldsymbol{K}_1\mathbf{Sig}^p(\boldsymbol{e}) - \boldsymbol{e}^T\boldsymbol{K}_2\mathbf{Sig}^q(\boldsymbol{e})\\
&= -\sum_{i=1}^{n} k_{1i}|e_i|^{p+1} - \sum_{i=1}^{n} k_{2i}|e_i|^{q+1}\\
&= -\sum_{i=1}^{n} k_{1i}\left(\|\boldsymbol{e}\|^2\right)^{\frac{p+1}{2}} - \sum_{i=1}^{n} k_{2i}\left(\|\boldsymbol{e}\|^2\right)^{\frac{q+1}{2}}.
\end{aligned}
\tag{58}
$$

Because of $0 < p < 1$, $q > 1$, we have $0 < \frac{p+1}{2} < 1$ and $\frac{q+1}{2} > 1$. From Lemma 2, (58) can be verified as

$$
\dot{V}_2 \leqslant -\lambda_{\min}(\boldsymbol{K}_1)\|\boldsymbol{e}\|^{p+1} - \lambda_{\min}(\boldsymbol{K}_2)n^{\frac{1-q}{2}}\|\boldsymbol{e}\|^{q+1}. \tag{59}
$$

Substituting (57) into (59) yields

$$
\dot{V}_2 + 2^{\frac{p+1}{2}}\lambda_{\min}(\boldsymbol{K}_1)V_2^{\frac{p+1}{2}} + 2^{\frac{q+1}{2}}\lambda_{\min}(\boldsymbol{K}_2)n^{\frac{1-q}{2}}V_2^{\frac{q+1}{2}} \leqslant 0. \tag{60}
$$

By using Lemma 1, the bound of sliding time T_s can be given by (46).

Case 2: If $\|\boldsymbol{e}\| < \delta$, (55) can be rewritten as

$$\dot{\boldsymbol{e}} = -l_1\boldsymbol{K}_1\boldsymbol{e} - l_2\boldsymbol{K}_1\mathbf{Sig}^2(\boldsymbol{e}) - l_3\boldsymbol{K}_1\boldsymbol{e}^3 - \boldsymbol{K}_2\mathbf{Sig}^q(\boldsymbol{e}). \tag{61}$$

Similarly, differentiating V_2 with respect to time and substituting (61) leads to

$$\begin{aligned}\dot{V}_2 &= \boldsymbol{e}^T\begin{pmatrix}-l_1\boldsymbol{K}_1\boldsymbol{e} - l_2\boldsymbol{K}_1\mathbf{Sig}^2(\boldsymbol{e})\\ -l_3\boldsymbol{K}_1\boldsymbol{e}^3 - \boldsymbol{K}_2\mathbf{Sig}^q(\boldsymbol{e})\end{pmatrix}\\ &= -\boldsymbol{K}_1\left(\frac{1}{2}p^2 - \frac{5}{2}p + 3\right)\delta^{p-1}\boldsymbol{e}^T\boldsymbol{e}\\ &\quad -\boldsymbol{K}_1\left(-p^2+4p-3\right)\delta^{p-2}\boldsymbol{e}^T\mathbf{Sig}^2(\boldsymbol{e})\\ &\quad -\boldsymbol{K}_1\left(\frac{1}{2}p^2 - \frac{3}{2}p + 1\right)\delta^{p-3}\boldsymbol{e}^T\boldsymbol{e}^3 - \boldsymbol{K}_2\boldsymbol{e}^T\mathbf{Sig}^q(\boldsymbol{e})\\ &= -\boldsymbol{K}_1V_2\delta^{p-1}\\ &\quad \cdot\left[\begin{array}{c}\underbrace{p^2-5p+6+2^{\frac{3}{2}}V_2^{\frac{1}{2}}\left(-p^2+4p-3\right)\delta^{-1}}_{\varphi_1(p)}\\ \underbrace{+V_2\left(2p^2-6p+4\right)\delta^{-2}}_{\varphi_2(p)}\end{array}\right]\\ &\quad -\boldsymbol{K}_2\boldsymbol{e}^T\mathbf{Sig}^q(\boldsymbol{e}).\end{aligned} \tag{62}$$

According to $V_2 = \frac{1}{2}\boldsymbol{e}^T\boldsymbol{e}$ and $\|\boldsymbol{e}\| < \delta$, it is easy to obtain that $0 \leqslant 2^{\frac{3}{2}}V_2^{\frac{1}{2}}\delta^{-1} < 2$. Since $\|\boldsymbol{e}\| < \delta$ and $0 < p < 1$, we have

$$\begin{aligned}\varphi_1(p) &> p^2 - 5p + 6 + 2\left(-p^2+4p-3\right)\\ &= -p^2 + 3p > 0,\end{aligned} \tag{63}$$

$$\varphi_2(p) = 2V_2\left(p^2 - 3p + 2\right)\delta^{-2} > 0. \tag{64}$$

Further simplification of $\dot{V}_2$ yields

$$\begin{aligned}\dot{V}_2 &< -\boldsymbol{K}_2\boldsymbol{e}^T\mathbf{Sig}^q(\boldsymbol{e}) = -\sum_{i=1}^{n}k_{2i}|e_i|^{q+1}\\ &\leqslant -n^{\frac{1-q}{2}}\lambda_{\min}(\boldsymbol{K}_2)\|\boldsymbol{e}\|^{q+1}.\end{aligned} \tag{65}$$

Substituting the Lyapunov function given by (57) into (65), we have

$$\dot{V}_2 + 2^{\frac{q+1}{2}}n^{\frac{1-q}{2}}\lambda_{\min}(\boldsymbol{K}_2)V_2^{\frac{1+q}{2}} \leqslant 0. \tag{66}$$

According to Lyapunov stability theory [41], the trajectory tracking error can converge to zero exponentially when $\|\boldsymbol{e}\| < \delta$.

This completes our proof. □

Remark 10: The proposed controller parameters should be carefully chosen by the following principles. First, constants m_1 and m_2 should be chosen to satisfy the inequality (36); otherwise, it can lead to chattering of the control torque. Then, based on m_1 and m_2, we can obtain γ by (35). Further, depending on the amplitude of the model uncertainty and bounded external disturbances, we can choose the constants b_0, b_1 and b_2 such that the coupling uncertainty satisfies the upper bound (38). For the other control parameters $\boldsymbol{K}_0$, $\boldsymbol{K}_1$, $\boldsymbol{K}_2$, $r > 1$, $k > 0$, $0 < p < 1$, $0 < \delta \leqslant 1$ and $q > 1$, they should be chosen by trial-and-error for a good tracking performance. Generally, δ should be chosen as small as possible to ensure the convergence accuracy of the system. Smaller p contributes to fast transient response, and q should be chosen as small as possible, they can have a significant effect on the control torque and should be modified carefully. Larger control gains $\boldsymbol{K}_0, \boldsymbol{K}_1, \boldsymbol{K}_2$, and k contribute to faster convergence of the system; hence they can be selected as large as possible within the range required to satisfy the system torque.

Remark 11: It is worth noting that the discontinuous term $\boldsymbol{\tau}_2$ in (33) can induce chattering in practical application. Generally, the boundary layer method is applied to reduce the chattering of the system [42], i.e., (33) is modified to

$$\boldsymbol{\tau}_2 = -\frac{\boldsymbol{s}}{\|\boldsymbol{s}\| + s_0}u, \tag{67}$$

where s_0 is a small positive constant and it can be defined as 5×10^{-3}.

4. SIMULATION RESULTS

To verify the effectiveness of the proposed FCFSMC scheme, a two-link robotic manipulator in the configuration shown in Fig. 6 is used.

To compare the performance of the proposed control scheme fairly with existing control schemes, the dynamic model of the two-link manipulator is chosen to be the same as that in the works of Yang *et al.* [9], Su *et al.* [31] and Zhang *et al.* [32]. The dynamics of the robotic manipulator are denoted as

$$\begin{aligned}&\begin{bmatrix}M_{11}(q) & M_{12}(q)\\ M_{21}(q) & M_{22}(q)\end{bmatrix}\begin{bmatrix}\ddot{q}_1\\ \ddot{q}_2\end{bmatrix} + \begin{bmatrix}C_{11}(q) & C_{12}(q)\\ C_{21}(q) & C_{22}(q)\end{bmatrix}\begin{bmatrix}\dot{q}_1\\ \dot{q}_2\end{bmatrix}\\ &\quad + \begin{bmatrix}G_1(q)\\ G_2(q)\end{bmatrix} = \begin{bmatrix}\tau_1\\ \tau_2\end{bmatrix},\end{aligned} \tag{68}$$

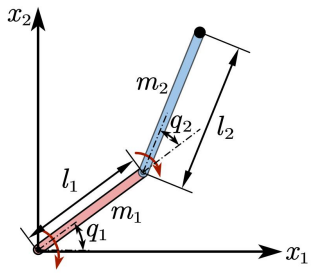

Fig. 6. Architecture of the two-link robotic manipulator.

Table 1. Controller parameters of the FCFSMC.

Parameter	Value
Positive constant δ	0.01
Positive constant q	1.5
Lower bound m_1	0.09
Upper bound m_2	0.2
Gain constant k	1
Gain matrices $\boldsymbol{K}_0, \boldsymbol{K}_1, \boldsymbol{K}_2$	$2I_2$
Positive constant p	0.5
Positive constant r	1.2
Positive constant b_0	12
Positive constant b_1	2.2
Positive constant b_2	2.8

where

$$
\begin{aligned}
&M_{11}(q) = (m_1+m_2)l_1^2+m_2l_2^2+2m_2l_1l_2\cos(q_2)+I_1,\\
&M_{12}(q) = M_{21}(q) = m_2l_2^2+m_2l_1l_2\cos(q_2),\\
&M_{22}(q) = m_2l_2^2+I_2,\\
&C_{11}(q,\dot{q}) = -2m_2l_1l_2\sin(q_2)\dot{q}_2,\\
&C_{12}(q,\dot{q}) = -m_2l_1l_2\sin(q_2)\dot{q}_2,\\
&C_{21}(q,\dot{q}) = m_2l_1l_2\sin(q_2)\dot{q}_1,\\
&C_{22}(q,\dot{q}) = 0,\\
&G_1(q) = (m_1+m_2)gl_1\cos(q_1)+m_2gl_2\cos(q_1+q_2),\\
&G_2(q) = m_2l_2g\cos(q_1+q_2).
\end{aligned}
$$

The dynamic model parameters of the robotic manipulator are set as: $l_1 = 1$ m, $l_2 = 0.8$ m, $m_1 = 0.5$ kg, $m_2 = 1.5$ kg, $I_1 = I_2 = 5$ kg $\cdot$ m^2, where l_i, m_i, and I_i are the length, mass, and inertia of link i, respectively with $i = 1, 2$, and $g = 9.81$ m/s^2 is the acceleration due to gravity. The nominal values of m_1, m_2 are defined as $m_1^0 = 0.6$ kg, $m_2^0 = 1.8$ kg, and the nominal values of I_1, I_2 are $I_1^0 = 6$ kg $\cdot$ m^2, $I_2^0 = 6$ kg $\cdot$ m^2.

The reference trajectories of the robotic manipulator $q_d = [q_{d1}, q_{d2}]^T$ are set the same as those in [9,31,32], with

$$
\begin{aligned}
q_{d1} &= 1.25-\frac{7}{5}\exp(-t)+\frac{7}{20}\exp(-4t),\\
q_{d2} &= 1.25+\exp(-t)-\frac{1}{4}\exp(-4t).
\end{aligned}
\tag{69}
$$

Simultaneously, the initial conditions of the robotic manipulator system are set as $q_1(0) = 1, q_2(0) = 1.5, \dot{q}_1(0) = 0, \dot{q}_2(0) = 0$. The parameters of the proposed controller are listed in Table 1.

To fully reflect the performance of different control schemes, all the simulations in this paper are assumed that the control torque output by the controller is achievable, that is, the output control torque does not exceed the upper bound of the allowable control torque of the joint. Two sets of comparative simulation results are described in this section to illustrate the effectiveness and superiority of the proposed approach compared to the Fixed TSMC, singularity-free fixed-time sliding mode control (SFSMC), and TSMC schemes. All the simulations are conducted using the Simulink of Matlab 2018b, with a time step size of 1×10^{-5}.

4.1. Comparison of control performance with Fixed TSMC

The Fixed TSMC scheme, proposed in the work of Su *et al.* [31], can be described as

$$
\begin{aligned}
&\boldsymbol{\tau} = \boldsymbol{\tau}_0+\boldsymbol{\tau}_1+\boldsymbol{\tau}_2,\\
&\boldsymbol{\tau}_0 = \boldsymbol{M}_0(\boldsymbol{q})\ddot{\boldsymbol{q}}_d+\boldsymbol{C}_0(\boldsymbol{q},\dot{\boldsymbol{q}})\dot{\boldsymbol{q}}+\boldsymbol{G}_0(\boldsymbol{q}),\\
&\boldsymbol{\tau}_1 = -\boldsymbol{K}_0\mathbf{Sig}^r(\boldsymbol{s}_1)\\
&\qquad -\boldsymbol{M}_0(\boldsymbol{q})\left(\boldsymbol{K}_1\boldsymbol{F}^p(\boldsymbol{e})+\boldsymbol{K}_2\boldsymbol{H}^q(\boldsymbol{e})\right)\dot{\boldsymbol{e}}\\
&\boldsymbol{\tau}_2 = -\frac{\boldsymbol{s}_1}{\|\boldsymbol{s}_1\|+s_0}\frac{1}{1-\gamma}\begin{pmatrix}k+b_0+b_2\|\dot{q}\|^2\\+\gamma\|\boldsymbol{\tau}_0+\boldsymbol{\tau}_1\|\end{pmatrix},
\end{aligned}
\tag{70}
$$

where the sliding mode surface $\boldsymbol{s}_1$ is described in (27), and the other parameters are denoted by (32)-(34). A faster convergence rate is always desired in tracking control, and a smaller p is helpful to accelerate the convergence; thus, $p = 0.2$ is chosen for this comparison. Defining the parameter $\delta_1 = 0.01$ and the other system parameters of the Fixed TSMC are the same as shown in Table 1. Except for the parameter p, the other parameters are also the same as those in [31]. Figs. 7 and 8 display the simulation results of trajectory tracking under controllers (30)-(34) and (70), respectively.

Fig. 7 represents the trajectory-tracking response of FCFSMC and Fixed TSMC with $p = 0.2$. It can be seen that the tracking response driven by FCFSMC provides a faster convergence rate than that of Fixed TSMC. This is because the proposed sliding mode surface has a faster error convergence rate when the tracking error is close to zero. Fig. 8 shows the control torque, where we can see that there are two saltations in the control torque of Fixed TSMC at $t_1 = 0.6407$ s and $t_2 = 0.7736$ s. This is

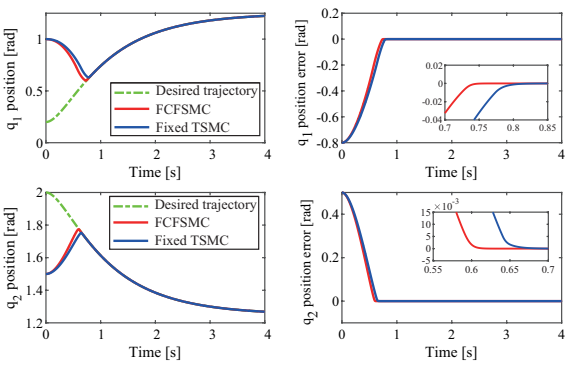

Fig. 7. Position-tracking trajectories and position tracking errors of FCFSMC and Fixed TSMC with $p = 0.2$.

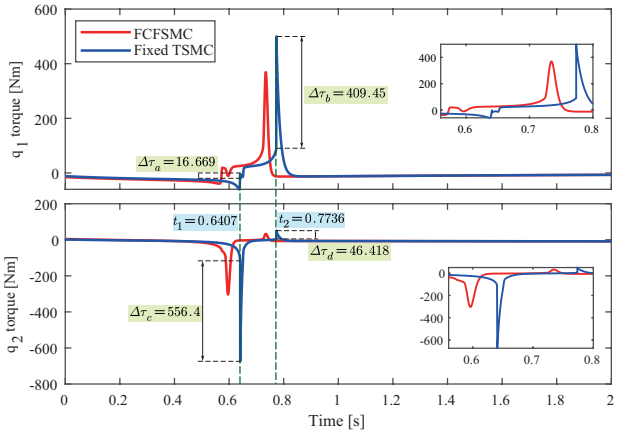

Fig. 8. Control input torque of FCFSMC and Fixed TSMC with $p = 0.2$.

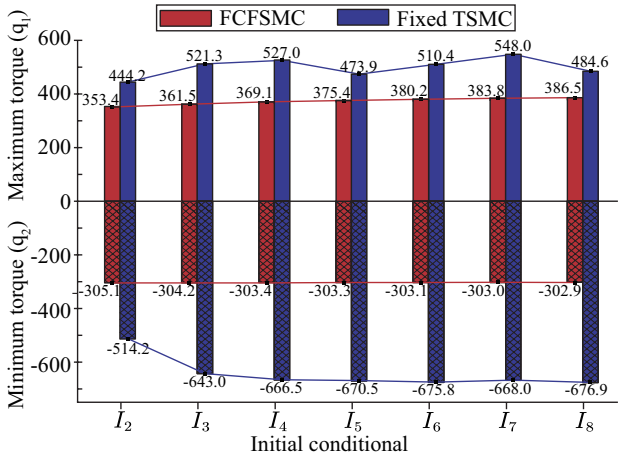

Fig. 9. Comparison of the maximum torque of q_1 and the minimum torque of q_2 of FCFSMC and Fixed TSMC with $p = 0.2$.

Table 2. Different initial positions and errors.

	$[q_1(0), q_2(0)]$	Initial error		$[q_1(0), q_2(0)]$	Initial error
I_1	[0.20, 2.00]	[0, 0]	I_5	[1.25, 1.25]	[-1.05, 0.75]
I_2	[0.50, 1.80]	[-0.30, 0.20]	I_6	[1.50, 1.00]	[-1.30, 1.00]
I_3	[0.75, 1.65]	[-0.55, 0.35]	I_7	[1.75, 0.75]	[-1.55, 1.25]
I_4	[1.00, 1.50]	[-0.80, 0.50]	I_8	[2.00, 0.50]	[-1.80, 1.50]

due to the discontinuity of $s_1^{p'}(x)$, as explained in Remark 5. The maximin transient control torque variable quantities are $\Delta\tau_b = 409.45$ Nm in q_1, and $\Delta\tau_c = 556.4$ Nm in q_2. In contrast, the control torque of FCFSMC is continuous, which implies that the proposed controller will not cause chattering of the robotic manipulator. Moreover, it can also obtain that FCFSMC is less prone to actuator saturation and more acceptable for engineering applications.

A stable control torque range means that the system can maintain similar maximum and minimum control torques in different initial states. To compare the influence of the initial condition on the control torque, the robotic manipulator in different initial states are set, and the control torque is simulated with FCFSMC and Fixed TSMC. Eight different initial joint angles are listed in Table 2. Fig. 9 shows the maximum control torque of joint 1 and the minimum control torque of joint 2 in FCFSMC and Fixed TSMC with different initial conditions $I_2 - I_8$. From Fig. 9, we can calculate the maximum absolute value of the control torque q_1 in FCFSMC as 70.53 % of that in Fixed TSMC, and q_2 is approximately 45.07 %. For q_1, the change in the maximum control torque in FCFSMC is 9.37 %, and the change in the maximum control torque in Fixed TSMC is 23.37 %, and the changes in FCFSMC and Fixed TSMC for q_2 are 0.73 % and 31.6 %, respectively. It can be concluded from the comparisons that the proposed control scheme is more robust under different initial conditions.

4.2. Comparison of control performance with SFSMC and NFTSMC

The SFSMC scheme was designed in the work of Zhang *et al.* [32] as

$$
\begin{aligned}
&\boldsymbol{F}(\boldsymbol{e}) = [f(e_1), \cdots, f(e_n)]^T,\\
&\boldsymbol{B}(\boldsymbol{e}) = \operatorname{diag}\left\{s_2^{p'}(e_i)\right\},\ i = 1,\ \cdots,\ n,\\
&\boldsymbol{D}^{\boldsymbol{r}}(\boldsymbol{x}) = \operatorname{diag}\{|e_i|^r\},\ i = 1,\ \cdots,\ n,\\
&\boldsymbol{\tau} = -\boldsymbol{\eta} + \boldsymbol{\tau}_0 + \boldsymbol{\tau}_1,\\
&\boldsymbol{\eta} = \boldsymbol{K}_1\boldsymbol{M}_0(\boldsymbol{q})\boldsymbol{B}(\boldsymbol{e})\dot{\boldsymbol{e}} + \boldsymbol{K}_2\boldsymbol{M}_0(\boldsymbol{q})\boldsymbol{D}^{\beta-1}(\boldsymbol{e})\dot{\boldsymbol{e}}\\
&\qquad -\boldsymbol{C}_0(\boldsymbol{q},\dot{\boldsymbol{q}})\dot{\boldsymbol{q}} - \boldsymbol{G}_0(\boldsymbol{q}) - \boldsymbol{M}_0(\boldsymbol{q})\ddot{\boldsymbol{q}}_{\boldsymbol{d}},\\
&\boldsymbol{\tau}_0 = -\boldsymbol{K}_3\mathbf{Sig}^{v_1}(\boldsymbol{s}_2) - \boldsymbol{K}_4\mathbf{Sig}^{v_2}(\boldsymbol{s}_2),\\
&\boldsymbol{\tau}_1 = -\mathbf{sgn}(\boldsymbol{s}_2)\frac{1}{1-\gamma}\left(b_0 + b_1\|\dot{\boldsymbol{q}}\|^2 + \gamma\|\boldsymbol{\tau}_0 - \boldsymbol{\eta}\|\right),
\end{aligned}
\tag{71}
$$

where β, v_1, v_2 are some known positive constants, with $\beta > 1$, $v_1 > 1$, $0 < v_2 < 1$. $\boldsymbol{K}_3$, $\boldsymbol{K}_4 \in \mathbb{R}^{n\times n}$ denote two positive-definite diagonal matrices, and the sliding mode surface $\boldsymbol{s}_2$ is defined in (29). $\boldsymbol{K}_1$, $\boldsymbol{K}_2$, γ, b_0, b_1 can be considered the same as in the proposed control scheme. In accordance with [32], the parameters of SFSMC are defined as $\boldsymbol{K}_3$, $\boldsymbol{K}_4 = 5\boldsymbol{I}_2$, $v_1 = 2.5$, $v_2 = 0.5$, $\delta_2 = 0.3$ and $\beta = 1.9$, and the other parameters are the same as those listed in Table 1.

As described in the work of Yang *et al.* [9], the NFTSMC is given as

$$
\begin{aligned}
&\boldsymbol{s}_3 = \boldsymbol{e} + \mathbf{Sig}^{\boldsymbol{\Gamma}_1}(\boldsymbol{e}) + \mathbf{Sig}^{\boldsymbol{\Gamma}_2}(\dot{\boldsymbol{e}}),\\
&\zeta = \left\|\boldsymbol{M}_0^{-1}(\boldsymbol{q})\right\|\left(b_0 + b_1\|\boldsymbol{q}\| + b_2\|\dot{\boldsymbol{q}}\|^2\right),\\
&\boldsymbol{F}_2 = -\boldsymbol{M}_0^{-1}(\boldsymbol{q})\left(\boldsymbol{C}(\boldsymbol{q},\dot{\boldsymbol{q}}) + \boldsymbol{G}_0(\boldsymbol{q})\right) - \ddot{\boldsymbol{q}}_{\boldsymbol{d}},
\end{aligned}
$$

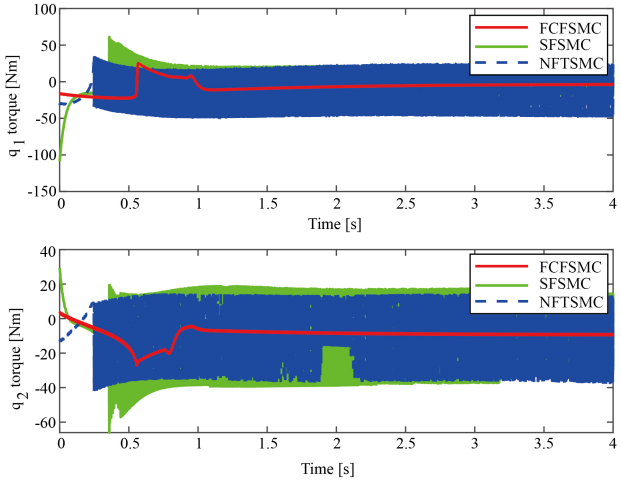

Fig. 10. Position tracking trajectories and position tracking errors.

$$\boldsymbol{\tau} = -\boldsymbol{M_0}(\boldsymbol{q}) \begin{bmatrix} M_2 \boldsymbol{s}_3 + (\zeta + M_1) \frac{\boldsymbol{s}_3}{\|\boldsymbol{s}_3\|} + \boldsymbol{F}_2 \\ +\boldsymbol{\Gamma}_2^{-1} \left(\boldsymbol{I}_2 + \boldsymbol{\Gamma}_1 D^{\boldsymbol{\Gamma}_1 - \boldsymbol{I}_2}(\boldsymbol{e}) \right) \\ \cdot \mathbf{Sig}^{2\boldsymbol{I}_2 - \boldsymbol{\Gamma}_2}(\dot{\boldsymbol{e}}) \end{bmatrix}, \tag{72}$$

where $M_1, M_2 \in \mathbb{R}$ are two positive constants, $\boldsymbol{\Gamma}_1$ and $\boldsymbol{\Gamma}_2$ are two positive-definite diagonal matrices, $D^{\boldsymbol{\Gamma}_1 - \boldsymbol{I}_2}(\boldsymbol{e})$ is denoted as $\mathrm{diag}\left\{ |e_i|^{\Gamma_i - 1} \right\}$, and b_0, b_1, b_2 are the same as those in (34). In accordance with Yang *et al.* [9], the parameters of NFTSMC are defined as $\boldsymbol{\Gamma}_1 = \mathrm{diag}\{2, 2\}$, $\boldsymbol{\Gamma}_2 = \mathrm{diag}\{\frac{5}{3}, \frac{5}{3}\}$, and $M_1 = M_2 = 2$. For a fair comparison, the parameters of both of the above control schemes are the same as those given in [9,32].

To evaluate the control performance of the proposed controller with external disturbances, the disturbances are set the same as in [32], with $\boldsymbol{\tau_d} = \left[2\sin(t) + 0.5\sin(200\pi t) \;\; \cos(2t) + 0.5\sin(200\pi t)\right]^T$.

The position-tracking trajectories and tracking errors are shown in Fig. 10. It can be observed that the proposed controller has a faster convergence rate than that of the SFSMC and NFTSMC. Moreover, the SFSMC has a fast convergence rate with a large position error, but the convergence rate decreases rapidly as the tracking errors converge. This arises from the properties of the nonlinear function $s_2^p(x)$, as described previously.

As shown in Fig. 11, it can be seen that the control torque curve of FCFSMC remains smooth without chattering, and SFSMC and NFTSMC have strong chattering caused by the discontinuous term in the controller. In essence, chattering in SFSMC and NFTSMC is caused by the signum function. In addition, the range of the control torque of the SFSMC scheme is larger than that of the proposed control scheme. In the SFSMC scheme, both the maximum control torque and the minimum control torque significantly exceed the torque value in the proposed control scheme. This is because the SFSMC scheme

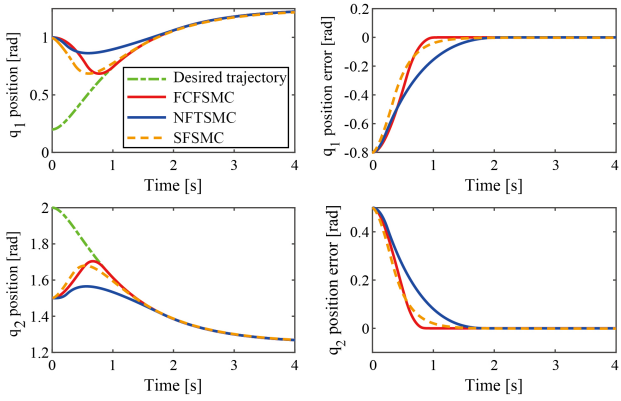

Fig. 11. Control input torque.

has a large initial control torque, as described in Remark 6. Thus, the proposed controller is less likely to cause actuator saturation and is easier to be applied in robotic manipulators.

4.3. Comparative study

For an obvious comparison, the performance of the control torque change can be evaluated by the total variation (TV), which can be expressed as [43]

$$\mathrm{TV} = \sum_{i=1}^{N-1} |\tau_{i+1} - \tau_i|. \tag{73}$$

In addition, the position tracking error index of the manipulator can be evaluated by the mean absolute error (MAE). The energy consumption index of the controller can be evaluated by the function related to torque, i.e., [44]

$$\mathrm{E} = \int_0^t \tau^T \tau dt. \tag{74}$$

A thorough comparison of the numerical simulations with the above-mentioned methods is given in Table 3. It reveals that, compared with the Fixed TSMC scheme, the proposed control scheme has a faster convergence rate, a smaller control torque range, less chattering and better tracking performance, and they consume almost the same amount of energy. In particular, the proposed control scheme has an obvious advantage when p decreases. Compared with the SFSMC and NFTSMC schemes, the proposed control scheme has a significantly faster convergence rate. In addition, SFSMC has the largest control torque range, owing to the large initial torque. The control torque range of the NFTSMC can be attributed to the chattering. Due to the chattering of the control system, the value of TV and the energy consumption of the SFSMC and NFTSMC schemes are much larger than that of the proposed control scheme. The value of MAE of the NFTSMC is the largest, while the other three control schemes have approximate tracking errors. It is worth noting that external disturbances have little effect on the convergence time and control torque range of the proposed

Table 3. Comparison results of the three control schemes.

Disturbance	p	Controller	Setting time T (s, $e < 10^{-4}$)		Control torque (Nm)		TV	MAE	E
			q_1	q_2	q_1	q_2			
N	0.2	FCFSMC	0.754	0.615	[-39.2 369.0]	[-303.8 33.0]	1572.4	0.0663	3.59×10^{8}
	0.2	Fixed TSMC	0.832	0.686	[-59.9 499.6]	[-674.1 50.8]	2631.5	0.0712	3.86×10^{8}
	0.5	FCFSMC	1.056	0.908	[-22.6 25.8]	[-26.7 2.3]	164.9	0.0722	8.30×10^{7}
	0.5	Fixed TSMC	1.186	1.043	[-19.2 24.5]	[-32.0 -0.1]	206.8	0.0777	7.58×10^{7}
Y	0.5	FCFSMC	1.057	0.902	[-22.9 25.4]	[-27.2 3.7]	1.16×10^{3}	0.0718	8.33×10^{7}
	0.5	Fixed TSMC	1.194	1.038	[-19.6 23.7]	[-32.3 1.3]	1.30×10^{3}	0.0772	7.59×10^{7}
	-	SFSMC	2.541	2.390	[-108.9 61.1]	[-66.1 29.3]	2.31×10^{7}	0.0694	3.47×10^{8}
	-	NFTSMC	2.094	1.835	[-49.9 35.0]	[-42.0 14.7]	1.51×10^{7}	0.1000	3.35×10^{8}

control scheme, which implies that the proposed control scheme has good anti-interference performance.

In summary, through the above comparative analysis of the data in Table 3, compared with the existing finite-time SMC scheme and fixed-time SMC schemes, the advantages of the proposed control scheme can be emphasized as follows:

1) Compared with the finite-time SMC, such as NFTSMC, the proposed fixed-time SMC scheme has a significant advantage in that the upper bound of the settling time is independent of the initial state of the system. This feature makes the proposed control scheme more suitable for manipulator systems with error convergence time constraints. In addition, a faster error convergence rate and higher precision tracking error are also advantaging over the finite-time SMC.

2) Compared with the existing fixed-time SMC schemes, such as SFSMC and Fixed TSMC, the proposed control scheme has a smoother control torque that can reduce the chattering of the robotic manipulator. With the boundary-layer technology, the chattering and energy consumption of the proposed control scheme is far less than those of SFSMC. Considering the same boundary-layer technology, it has higher tracking accuracy and a more stable control torque range at different initial positions than those of the Fixed TSMC.

It is worth mentioning that in addition to the above discussion, the advantage of the proposed controller over the traditional proportional-integral-differential (PID) control as well as neural network control is its strong robustness to external disturbances and the convergence error bound independent of the initial state of the system. The proposed control scheme is more suitable for scenarios requiring higher performance for robotic manipulators tracking control, and is also more easily applied than intelligent control algorithms.

5. EXPERIMENTAL RESULTS

In this section, the proposed FCFSMC scheme is further validated with several experimental results on a collaborative robotic manipulator. The robotic manipulator system is shown in Fig. 12 and the experiment platform consisted of a monitoring computer, a power supply, a cSPACE control platform with a digital signal processor (DSP, TMS320F28335) running as the controller and a 6-DOF collaborative robotic manipulator. The torque applied to the robotic manipulator is obtained by proportional conversion through the current generated by the controller. The feedback position of the joint is detected by a 17-bit absolute encoder with an accuracy of $\pm0.015^{\circ}$, and the joint velocity is obtained by differential measurement of position. The robotic manipulator joint module uses a 101:1 gearbox with a maximum allowable load of 157 N and 54 N for joints 2 and 3, respectively. The control program can be written with the Simulink of Matlab 2018b, and the control schemes are applied to the robotic manipulator by the following steps. First, the proposed control algorithm is offline programmed using MATLAB/Simulink (MATLAB R2018a or a higher version). Then, through the cSPACE control platform, the MATLAB/Simulink program is directly converted into C codes. Next, in the Code Composer Studio (CCS) software environment, the converted C codes are downloaded to the DSP control board of the controller through the simulator. Finally, the pro-

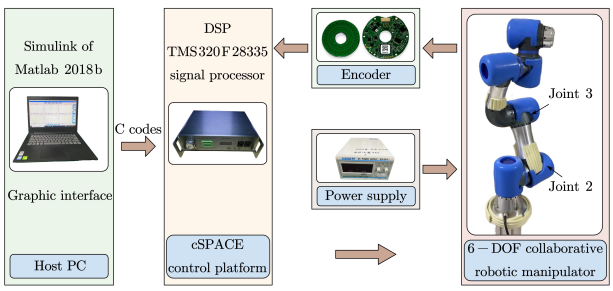

Fig. 12. Diagram of robotic manipulator system

posed control algorithm is employed by a DSP processor in the form of C codes in real-time, while the sample time is set as 5 ms.

In the experiment, joint 2 and joint 3 are used to verify the effectiveness of the proposed control scheme. According to the motor characteristics of the joints, the ranges of control torques are limited to $\boldsymbol{\tau}_{\max} = [157,\ 54]^T$ Nm. The desired trajectories given in the above simulation will converge to constants in a short time, so it is difficult to observe the tracking performance as the ideal trajectory changes. To compare the performance of control schemes more clearly, the desired trajectory is set as $\boldsymbol{q_d} = \left[\frac{\pi}{4}\sin(0.5t+0.1),\ 1.2-\exp(-0.1t)\right]^T$ (rad) and both the initial joint positions and velocities are set to zero. In order to illustrate the application value of the proposed control scheme, considering the above simulation results, we compare the proposed control method with the Fixed TSMC scheme [31] and the SFSMC scheme [32]. Based on the properties of the robotic manipulator, the upper bound parameters of the robotic manipulator are defined as $b_0 = 18$, $b_1 = 5$, $b_2 = 8$, $m_1 = 1.3$, and $m_2 = 2.1$. The gain parameters are chosen as $\boldsymbol{K}_0$, $\boldsymbol{K}_1$, $\boldsymbol{K}_2 = 1.2\boldsymbol{I}_2$ and $k = 1$ for the FCSMC and the Fixed TSMC. The parameters of SFSMC scheme are defined as $\boldsymbol{K}_3$, $\boldsymbol{K}_4 = 2\boldsymbol{I}_2$, $v_1 = 2.5$, $v_2 = 0.5$ and $\beta = 1.9$, and the other parameters are selected as shown in Table 1.

As a comparison, a PD controller based on gravity compensation is used as a comparator, whose control torque can be expressed as

$$\boldsymbol{\tau} = \boldsymbol{k_d}\dot{\boldsymbol{e}} + \boldsymbol{k_p}\boldsymbol{e} + \boldsymbol{G}_0(\boldsymbol{q}), \tag{75}$$

where $\boldsymbol{k_d}, \boldsymbol{k_p}$ are chosen as $\boldsymbol{k_p} = [200\ \ 0;\ 0\ 200]$, $\boldsymbol{k_d} = [100\ \ 0;\ 0\ \ 80]$.

Remark 12: In the SFSMC scheme, the sign function in the control torque τ_1 can cause strong chattering of the robotic manipulator, which may damage the manipulator. To eliminate the chattering caused by the discontinuous control in the SFSMC scheme [32], and to have a fair comparison with the proposed control scheme and the Fixed TSMC, the boundary-layer technology similar to the proposed control scheme was used in the experiment.

Fig. 13 shows the position-tracking trajectories and position-tracking errors comparisons. The experimental control inputs are shown in Fig. 14. Similar to the above simulation results, the SFSMC scheme [32] has a slightly slower convergence rate for tracking errors than the other two control schemes. For joint 2, the convergence time of tracking error of FCFSMC and Fixed-time TMSC schemes is about 1.4 s and about 1.2 s for joint 3. The convergence time of the SFSMC scheme is about twice of them. Compared to the SMC schemes, the PD controller has significantly worse tracking performance. The initial control torque in SFSMC scheme is larger than that in FCFSMC and Fixed-time TMSC scheme, which is consistent with the simulation results. Moreover, compared with the Fixed TSMC scheme [31], the Fixed TSMC scheme has two obvious torque chattering of about 3.06 N and 6.50 N at 0.74 s, and the control input torque of the proposed control scheme is smoother than others. It is worth mentioning that the control torque of the experimental results has chattering mainly due to the sensor of the robotic manipulator.

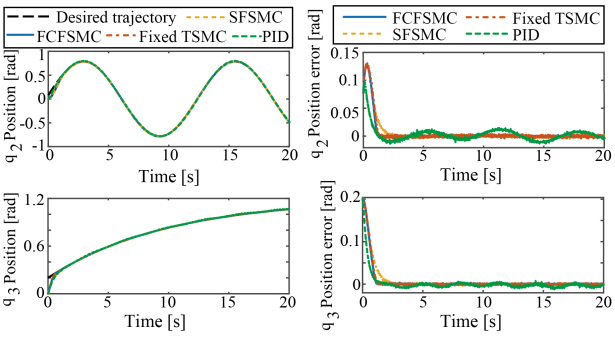

Fig. 13. Position-tracking trajectories and position-tracking errors.

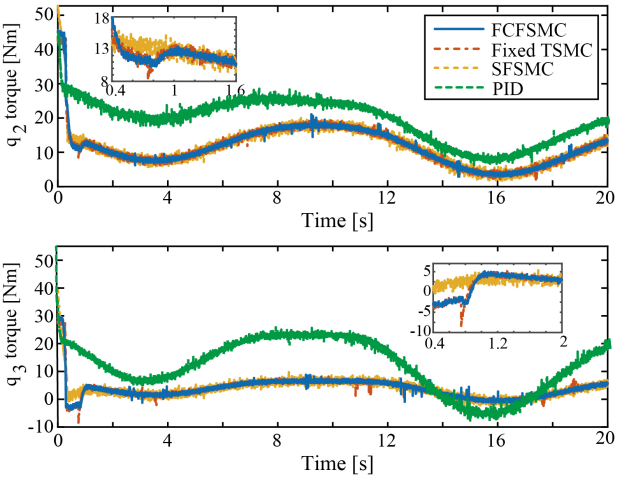

Fig. 14. Experimental control input torque.

6. CONCLUSION

In this work, a novel fast continuous fixed-time sliding mode surface and a fixed-time sliding mode control scheme are presented for an uncertain constrained n-link robotic manipulator. Combined with the Lyapunov stability technique, the proposed control scheme is analyzed and it is demonstrated that it can guarantee the convergence of position-tracking errors in a fixed time, irrespective of the initial conditions. Numerical simulations and experimental results show that transient changes in the control torque of robotic manipulators are eliminated using the proposed nonlinear function and the sliding mode surface. Compared with the existing fixed-time SMC and

finite-time SMC schemes, the proposed control scheme can provide a faster convergence rate with a smaller control torque range and higher trajectory tracking accuracy. Meanwhile, the extreme value of the control torque does not change greatly in different initial states of the manipulator system, which is beneficial to the application of the controller. In future work, the focus will be placed on finding a fixed-time control for uncertain robotic manipulators with a user-defined control torque range.

REFERENCES

[1] L. Roveda, M. Forgione, and D. Piga, "Robot control parameters auto-tuning in trajectory tracking applications," *Control Engineering Practice*, vol. 101, p. 104488, 2020.

[2] A.-A. S. Abdel-Salam and I. N. Jleta, "Fuzzy logic controller design for puma 560 robot manipulator," *IAES International Journal of Robotics and Automation*, vol. 9, no. 2, p. 73, 2020.

[3] G. Zheng, Y. Zhou, and M. Ju, "Robust control of a silicone soft robot using neural networks," *ISA Transactions*, vol. 100, pp. 38-45, 2020.

[4] Y. Wang, K. Zhu, B. Chen, and M. Jin, "Model-free continuous nonsingular fast terminal sliding mode control for cable-driven manipulators," *ISA Transactions*, vol. 98, pp. 483-495, 2020.

[5] S. Roy, S. Baldi, and L. M. Fridman, "On adaptive sliding mode control without a priori bounded uncertainty," *Automatica*, vol. 111, p. 108650, 2020.

[6] A. Ferrara, G. P. Incremona, and B. Sangiovanni, "Tracking control via switched integral sliding mode with application to robot manipulators," *Control Engineering Practice*, vol. 90, pp. 257-266, 2019.

[7] Y. Wu, X. Yu, and Z. Man, "Terminal sliding mode control design for uncertain dynamic systems," *Systems & Control Letters*, vol. 34, no. 5, pp. 281-287, 1998.

[8] Y. Feng, X. Yu, and Z. Man, "Non-singular terminal sliding mode control of rigid manipulators," *Automatica*, vol. 38, no. 12, pp. 2159-2167, 2002.

[9] L. Yang and J. Yang, "Nonsingular fast terminal sliding-mode control for nonlinear dynamical systems," *International Journal of Robust and Nonlinear Control*, vol. 21, no. 16, pp. 1865-1879, 2011.

[10] S. Yu, X. Yu, B. Shirinzadeh, and Z. Man, "Continuous finite-time control for robotic manipulators with terminal sliding mode," *Automaica*, vol. 41, pp. 1957-1964, 2005.

[11] M. Van, S. S. Ge, and H. Ren, "Finite time fault tolerant control for robot manipulators using time delay estimation and continuous nonsingular fast terminal sliding mode control," *IEEE Transactions on Systems, Man, and Cybernetics*, vol. 47, no. 7, pp. 1681-1693, 2017.

[12] P. Li, J. Ma, Z. Zheng, and L. Geng, "Fast nonsingular integral terminal sliding mode control for nonlinear dynamical systems," *Proc. of 53rd IEEE Conference on Decision and Control*, pp. 4739-4746, IEEE, 2014.

[13] M. Boukattaya, N. Mezghani, and T. Damak, "Adaptive nonsingular fast terminal sliding-mode control for the tracking problem of uncertain dynamical systems," *ISA Transactions*, vol. 77, pp. 1-19, 2018.

[14] S. Mondal and C. Mahanta, "Adaptive second order terminal sliding mode controller for robotic manipulators," *Journal of the Franklin Institute*, vol. 351, no. 4, pp. 2356-2377, 2014.

[15] S. Yi and J. Zhai, "Adaptive second-order fast nonsingular terminal sliding mode control for robotic manipulators," *Isa Transactions*, vol. 90, pp. 41-51, 2019.

[16] A. Polyakov, "Nonlinear feedback design for fixed-time stabilization of linear control systems," *IEEE Transactions on Automatic Control*, vol. 57, no. 8, pp. 2106-2110, 2011.

[17] A. Polyakov, D. Efimov, and W. Perruquetti, "Finite-time and fixed-time stabilization: Implicit lyapunov function approach," *Automatica*, vol. 51, pp. 332-340, 2015.

[18] Z. Zuo and L. Tie, "Distributed robust finite-time nonlinear consensus protocols for multi-agent systems," *International Journal of Systems Science*, vol. 47, no. 6, pp. 1366-1375, 2016.

[19] Z. Zuo and L. Tie, "A new class of finite-time nonlinear consensus protocols for multi-agent systems," *International Journal of Control*, vol. 87, no. 2, pp. 363-370, 2014.

[20] D. Gómez-Gutiérrez, "On the design of nonautonomous fixed-time controllers with a predefined upper bound of the settling time," *International Journal of Robust and Nonlinear Control*, vol. 30, no. 10, pp. 3871-3885, 2020.

[21] R. Aldana-López, D. Gómez-Gutiérrez, E. Jiménez-Rodríguez, J. D. Sánchez-Torres, and M. Defoort, "Enhancing the settling time estimation of a class of fixed-time stable systems," *International Journal of Robust and Nonlinear Control*, vol. 29, no. 12, pp. 4135-4148, 2019.

[22] L. Cao, B. Xiao, M. Golestani, and D. Ran, "Faster fixed-time control of flexible spacecraft attitude stabilization," *IEEE Transactions on Industrial Informatics*, vol. 16, no. 2, pp. 1281-1290, 2019.

[23] Y. Huang and Y. Jia, "Adaptive fixed-time relative position tracking and attitude synchronization control for noncooperative target spacecraft fly-around mission," *Journal of the Franklin Institute*, vol. 354, no. 18, pp. 8461-8489, 2017.

[24] A.-M. Zou, K. D. Kumar, and A. H. de Ruiter, "Fixed-time attitude tracking control for rigid spacecraft," *Automatica*, vol. 113, p. 108792, 2020.

[25] D. Zhou, A. Zhang, and P. Yang, "Fixed-time output feedback consensus of second-order multi-agent systems with settling time estimation," *International Journal of Control, Automation, and Systems*, vol. 18, pp. 2061-2074, 2020.

[26] Z. Zuo, "Nonsingular fixed-time consensus tracking for second-order multi-agent networks," *Automatica*, vol. 54, pp. 305-309, 2015.

[27] A.-M. Zou and W. Li, "Fixed-time output-feedback consensus tracking control for second-order multiagent systems," *International Journal of Robust and Nonlinear Control*, vol. 29, no. 13, pp. 4419-4434, 2019.

[28] Y. Li, L. Zhu, and Y. Guo, "Observer-based multivariable fixed-time formation control of mobile robots," *Journal of Systems Engineering and Electronics*, vol. 31, no. 2, pp. 403-414, 2020.

[29] X. Jin, "Adaptive fixed-time control for mimo nonlinear systems with asymmetric output constraints using universal barrier functions," *IEEE Transactions on Automatic Control*, vol. 64, no. 7, pp. 3046-3053, 2018.

[30] Y. Pan, P. Du, H. Xue, and H.-K. Lam, "Singularity-free fixed-time fuzzy control for robotic systems with user-defined performance," *IEEE Transactions on Fuzzy Systems*, vol. 29, no. 8, pp. 2388-2398, 2021.

[31] Y. Su, C. Zheng, and P. Mercorelli, "Robust approximate fixed-time tracking control for uncertain robot manipulators," *Mechanical Systems and Signal Processing*, vol. 135, p. 106379, 2020.

[32] L. Zhang, Y. Wang, Y. Hou, and H. Li, "Fixed-time sliding mode control for uncertain robot manipulators," *IEEE Access*, vol. 7, pp. 149750-149763, 2019.

[33] H. Sai, Z. Xu, S. He, E. Zhang, and L. Zhu, "Adaptive nonsingular fixed-time sliding mode control for uncertain robotic manipulators under actuator saturation.," *Isa Transactions*, vol. 123, pp. 46-60, 2022.

[34] Y. Hong, Y. Xu, and J. Huang, "Finite-time control for robot manipulators," *Systems & control letters*, vol. 46, no. 4, pp. 243-253, 2002.

[35] R. Courant and F. John, *Introduction to Calculus and Analysis I*, Springer Science & Business Media, 2012.

[36] E. Cruz-Zavala, E. Nu no, and J. A. Moreno, "Robust trajectory-tracking in finite-time for robot manipulators using nonlinear proportional-derivative control plus feedforward compensation," *International Journal of Robust and Nonlinear Control*, vol. 31, no. 9, pp. 3878-3907, 2021.

[37] M. W. Spong, S. Hutchinson, and M. Vidyasagar, *Robot Modeling and Control*, 2006.

[38] M. Zhihong and M. Palaniswami, "Robust tracking control for rigid robotic manipulators," *IEEE Transactions on Automatic Control*, vol. 39, no. 1, pp. 154-159, 1994.

[39] D. Cai, "Comments on "robust tracking control for rigid robotic manipulators"," *IEEE Transactions on automatic control*, vol. 43, no. 7, p. 1008, 1998.

[40] W.-H. Zhu, "Comments on "robust tracking control for rigid robotic manipulators"," *IEEE Transactions on Automatic Control*, vol. 45, no. 8, pp. 1577-1580, 2000.

[41] J.-J. E. Slotine and W. Li, *Applied Nonlinear Control*, 1991.

[42] P. Kachroo, "Existence of solutions to a class of nonlinear convergent chattering-free sliding mode control systems," *IEEE Transactions on automatic control*, vol. 44, no. 8, pp. 1620-1624, 1999.

[43] X. Liu and Y. Han, "Finite time control for mimo nonlinear system based on higher-order sliding mode," *ISA Transactions*, vol. 53, no. 6, pp. 1838-1846, 2014.

[44] H. Liu and T. Zhang, "Adaptive neural network finite-time control for uncertain robotic manipulators," *Journal of Intelligent and Robotic Systems*, vol. 75, no. 3, pp. 363-377, 2014.

Huayang Sai received a B.E. degree in School of Mechanical and Electronic Engineering form Northwest Agriculture and Forestry University, Yangling, China, in 2018. He is now a Ph.D. candidate in Mechanical Engineering and Automation, Changchun Institute of Optics, Fine Mechanics and Physics, Chinese Academy of Science, China. He is also currently pursuing the degree with the College of Optoelectronics, University of Chinese Academy of Sciences, Beijing. His current research interests include medical robot, robot impedance control.

Zhenbang Xu received the B.E. degree from the Department of Theoretical and Applied Mechanics, Chinese Academy of Sciences University, Hefei, China, in 2005, and the Ph.D. degree from the Chinese Academy of Sciences University, in 2010, where he is currently with the Changchun Institute of Optics, Fine Mechanics and Physics. His research interests include space intelligent robot, multi-dimensional precision adjustment mechanism, space structure dynamics, and microvibration control.

Enyang Zhang received the B.E. degree from the Department of Mechanical Engineering and Automation, Nanjing University of Aeronautics and Astronautics, Nanjing, China, in 2010, and the M.E. degree from Nanjing University of Aeronautics and Astronautics, in 2013, where he is currently with the Changchun Institute of Optics, Fine Mechanics and Physics. His research interests include space intelligent robot, and space structure dynamics.

Chunyang Han received the B.E. and M.S. degree from Jilin University, Changchun, China, in 2011, and the Ph.D.degree from the Chinese Academy of Sciences University, in 2020, where he is currently with the Changchun Institute of Optics, Fine Mechanics and Physics. His research interests include the structural design, mechanism research, simulation and experimental testing of the parallel robot and the space optical adjustment.

Yang Yu received the Ph.D. degree from the Changchun Institute of Optics, Fine Mechanics and Physics (CIOMP), Chinese Academy of Sciences (CAS) in 2016, where he is currently an associate researcher in the Changchun Institute of Optics, Fine Mechanics and Physics. His research interests include parallel robots, space intelligent robot.